THE JOURNAL OF PHYSICAL CHEMISTRY B

Article

pubs.acs.org/JPCB

Exploring the Proton Conductance and Drug Resistance of BM2 Channel through Molecular Dynamics Simulations and Free Energy Calculations at Different pH Conditions

Yuxin Zhang,[†,§] Hujun Shen,[†,§] Mingbo Zhang,[‡] and Guohui Li*[,†]

[†]Laboratory of Molecular Modeling and Design, State Key Laboratory of Molecular Reaction Dynamics, Dalian Institute of Chemical Physics, Chinese Academy of Sciences, Dalian, China 116023

[‡]College of Pharmacy, Liaoning University of Traditional Chinese Medicine, Dalian, 116600 China

Supporting Information

ABSTRACT: BM2 channel plays an important role in the replication of influenza virus B. However, few studies attempt to investigate the mechanism of the proton conductance in BM2 channel, as well as the drug resistance of the BM2 channel. The first experimental structure of the BM2 protein channel has recently been solved, enabling us to theoretically study BM2 systems with different protonation states of histidine. By performing molecular dynamics simulations on the BM2 systems with different protonation states of four His19 residues, we provided our understanding of the structure, dynamics, and drug resistance of the BM2 channel. In general, the results of our study and other investigations both have demonstrated that whether the BM2 channel adopts an open or a closed form depends on the protonation state of His19. Meanwhile, we discovered that a drug (amantadine) was unable to enter into the center of the BM2 channel even at a low pH condition probably due to the number of hydrophilic residues of the BM2 channel. Finally, potentials of mean force (PMF) calculations were performed for the drug binding BM2 channel, energetically explaining why the BM2 channel exhibited drug resistance to two inhibitors of the AM2 channel, amantadine and rimantadine.

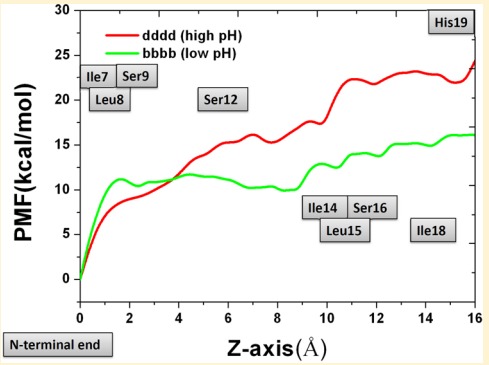

INTRODUCTION

The integral membrane protein of influenza virus A or B, AM2 or BM2, which is critical for the viral replication,[1−5] forms a proton channel, allowing protons to pass through the viral membrane under low pH conditions. BM2 is a functional homologue of AM2;[6] for instance, the proton conductance in the AM2 channel depends on the arrangement and flexibility of His37 and Trp41, whose counterparts in the BM2 channel are His19 and Trp23. Nevertheless, AM2 and BM2 channels have some substantial differences. First, BM2 exhibits coiled-coil characteristics with heptad repeats that allow the formation of a stable tetramer, while the cytoplasmic domain of AM2 is responsible for stabilizing the tetramer.[1,6−9] Second, except for the motif HxxxW, AM2 and BM2 show no sequence homology with each other.[1]

Nearly half of the influenza diseases in recent years were caused by influenza virus B, which almost exclusively infects humans.[2] Therefore, BM2 has been of great interest as a drug target. According to several previous reports, the AM2's inhibitors,[10,11] such as amantadine (AMT) and rimantadine (RMT), were both unable to inhibit BM2 proton conductance; for instance, Wang et al.[1] discovered that the proton conductance of the BM2 channel was completely insensitive to 50 μM of RMT, perhaps due to the different pore-lining residues facing the ectodomain between the two proteins.[12] However, the molecular mechanism of the drug resistance of BM2 is less well studied so far.

Currently, there are two dominant theories describing the molecular mechanism of the proton conductance in the AM2 channel. The first one, which is the so-called "shuttering" mechanism, states that the four histidine residues of the motif HxxxW region execute the function like a gate, and the channel is open due to the electric repulsion caused by the protonation of the histidine residues.[13,14] The other one, named the "shuttling" mechanism, suggests that the histidine residues are involved in the proton transfer;[15] that is, the imidazoles of histidines participate in conducting protons. For both theories, the formation of a water wire is necessary in the channel. However, the proton conductance in the BM2 channel is not well explored.

In this study, the high-resolution NMR structure of the BM2 transmembrane domain resolved by Wang et al.[1] was used as the initial structure for molecular dynamics (MD) simulations and free energy calculations. To investigate how the protonation state of His19 affects the pore size of the BM2 channel (see Figure 1), all possible protontation states of the

Received: September 29, 2012
Revised: November 25, 2012
Published: January 3, 2013

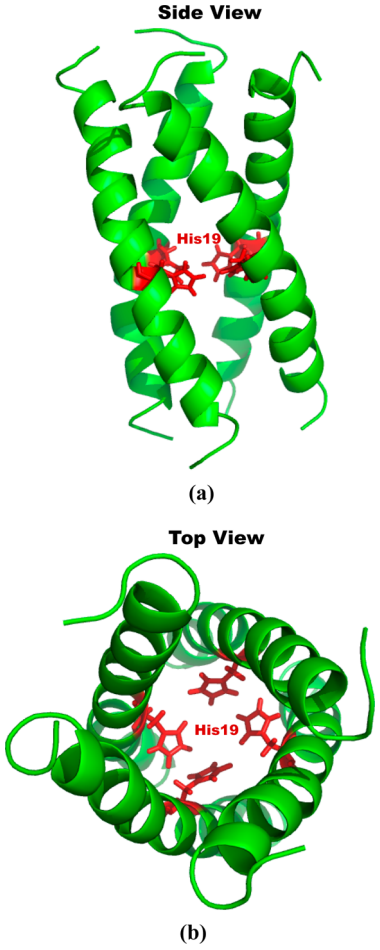

Figure 1. Side and top views of the homotetrameric helix bundles formed by the channel domain of BM2 protein from influenza B virus. The four His19 residues are indicated by red sticks.

four His19 residues were considered. Then, a total of 81 BM2 systems, which correspond to the BM2 channel under different pH conditions, were built and simulated for the first time. In addition, the potentials of mean force (PMF) calculations were performed on the BM2 channel bound by two drugs, AMT[16] and RMT[17] (see Figure S1 of the Supporting Information), in order to gain more understanding of the BM2 drug resistance.

METHODS

Building Models. The initial structure of BM2 was extracted from the NMR structure (PDB ID: 2KIX)[1] deposited in the protein data bank. There are three protonation states that can be assigned to each His19 residue in BM2, denoted with the symbols "b", "d", and "e", which correspond to protonated His19 at both ND1 and NE2 (HISb), at ND1 only (HISd), and at NE2 only (HISe), respectively (see Figure S1, Supporting Information). In this work, we have built 81 corresponding models (for instance, "bbbb", "bbbd", "bbbe", ..., "dddb", "dddd"), which contain all possible protonation states (corresponding to different pH conditions) of the four His19 residues. Using the inflating method, each system was inserted into the DOPC bilayer with 128 lipids, and finally, three lipids were removed for bad contacts with the protein.[18,19] Each was neutralized by adding chloride counterions, depending on the protonation states of the BM2 channel. Finally, TIP3P water molecules[20] were added, and the simulation box was set to 6.6 nm ×6.5 nm ×7.5 nm in size.

MD Simulations. All minimizations and MD simulations were carried out in the simulation package GROMACS.[21] The GROMOS96 53a6 force field was employed for all MD simulations, and the force field parameters of Berger et al. were applied to the lipid bilayer.[22] During the simulations, all bonds were constrained using the LINCS algorithm,[23] and the integration time step was set to 2 fs. The particle mesh Ewald (PME) method[24] was employed to treat long-range electrostatic interactions, and a cutoff value of 12 Å was used for nonbonded interactions.

Prior to the MD runs, all systems were minimized to remove the conflicting contacts. Then, the systems were heated to 310 K within 1 ns. For each system, a relaxation process of 1 ns for water molecules was performed by imposing a constraint on the protein and lipid with the force constant of 100000 KJ/mol/nm^2; then, the system was equilibrated for a further 10 ns with the constraint only imposed on the protein. Finally, removing all constraints applied to the system, the *NPT* simulation was performed for at least 30 ns.

Out of 81 systems, we selected two representative protonation states ("bbbb" and "dddd") that belong to 4+ and 0 states, respectively, because the "bbbb" state represents a very low pH condition and the "dddd" state corresponds to a high pH condition. For the two systems, the drug agent AMT was placed inside the BM2 pores near the N-terminal end. MD simulations were performed on the two systems at different pH conditions using the same simulation protocol described above. The structure of AMT was obtained from the crystal structure (PDB ID: 3C9J)[16] deposited in the protein data bank, and its force field parameters were calculated by PRODRG,[25] using the GROMOS96 force field.

PMF Calculations. PMF calculations[26−28] for the binding of AMT to the BM2 proton channel from the N-terminal end were performed at different pH conditions (the "bbbb" and "dddd" states of the BM2 channel). We first extracted 500 structures with an interval of 1 ps over the equilibrated trajectory of each MD simulation. From these 500 uncorrelated structures, 64 structures were randomly chosen as the windows for PMF calculation. Inside the BM2 channel, the AMT molecule was placed at 64 different positions along the channel axis from the N-terminal end to the vicinity of His19 at the interval of 0.25 Å. For each structure, a MD simulation of 10 ns was carried out with a force constant of 4000 KJ/mol/nm^2 imposed on the mass centers between the AMT and BM2 proton channels. The same procedure was applied to PMF calculations for the binding of RMT to the BM2 channel, and the structure of RMT was extracted from the Protein Data Bank (PDB ID: 2RLF).[17]

RESULTS/DISCUSSION

BM2 Channel, Sensitive to pH Conditions. The backbone RMSD curves of different BM2 systems against the simulation time have been plotted (see Figure S2 of the Supporting Information), indicating that all systems reached equilibrium within 20 ns; therefore, the subsequent MD simulations were considered as the production runs, from which the pore radii along each channel were calculated using the program HOLE2[29] (see Figure S3 of the Supporting Information). From the results of pore radii along the BM2 channels, we observed that in all cases, the motif HxxxW region was relatively narrower than other regions. Nevertheless, in

dx.doi.org/10.1021/jp309682t | J. Phys. Chem. B 2013, 117, 982−988

different protonation states of the BM2 channel, the motif HxxxW region exhibits distinct behaviors, indicating that the dynamics of the motif HxxxW region in the BM2 channel should vary with pH condition.

In order to demonstrate clearly how the protonation states of four His19 residues affect the pore size of the BM2 channel, the 81 BM2 systems were classified into five states, such as 4+, 3+, 2+, 1+, and 0+ states. For instance, the 4+ state indicates that four His19 residues are all protonated, and the 3+ state means that three out of four His19 residues are protonated, and so on. For each state (4+, 3+, 2+, 1+, and 0+), the pore radii along the proton channel helix were averaged over its own subsystems (such as "bbbb", "bbbd",...), and the comparison of the pore radii in different states is presented in Figure 2a. In general, the

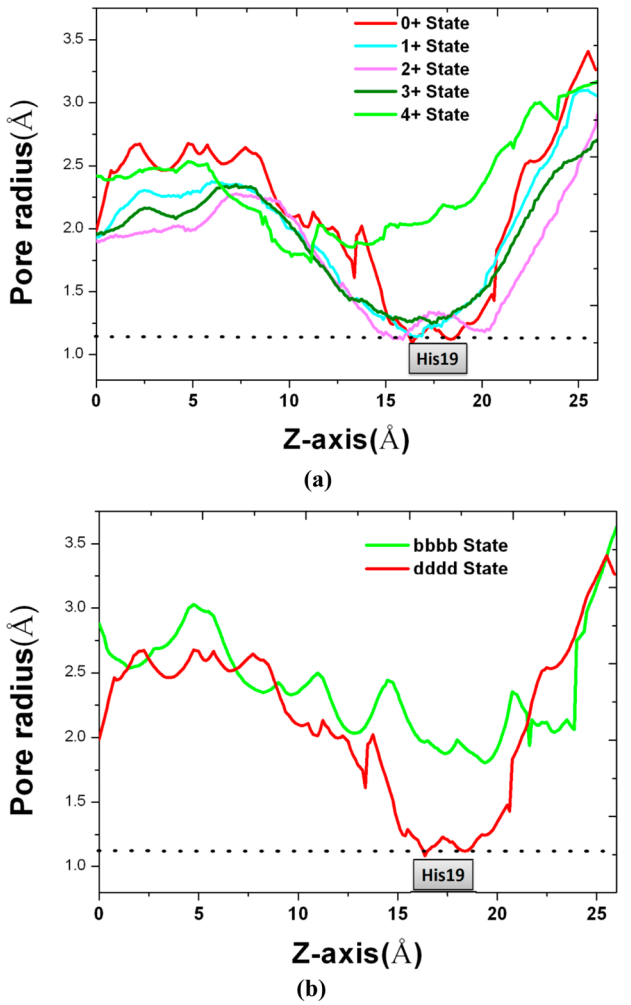

Figure 2. The pore radius profiles along the BM2 channel helix (Z-axis) in (a) different states (0+, 1+, 2+, 3+, 4+) indicated in different colors and (b) the "bbbb" (4+) and "dddd" states (0+), obtained from the equilibrated MD simulations. The radius of a water molecule is represented by a dotted line.

proton channel gate composed of four His19 residues started to open when the number of protonated His19 residues was increased to 3 (such as the 3+ state). When all four His19 residues were protonated (such as the 4+ state), the proton channel gate was widely open such that water molecules were allowed to freely move back and forth inside the channel. With the aid of coarse-grained and atomistic MD simulations, Rouse et al.[2] suggested that the BM2 channel gate was closed when no more than two of the four His19 residues were protonated and was open if three or four His19 residues were protonated. Therefore, our studies basically reached the same conclusion. Nevertheless, as for the 3+ (such as "ebbb", "edbb", etc.) or 2+ (such as "bddb", "bedd", etc.) states, their subsystems demonstrated that the His19 gate was open or closed in response to the specific protonation state of each His19 residue; see Figure S3 of the Supporting Information. For instance, in the case of the 2+ state (two His19 residues are protonated), the His19 gate may be open or closed depending on whether the two His19 moieties are adjacent or opposite. Therefore, one should be careful to conclude that the His19 gate is open if three His19 residues are protonated, and the His19 gate is closed if two His19 residues are protonated. Similar to the AM2 channel,[30] the open gate of the BM2 channel is the consequence of the electrostatic repulsion between the histidine residues being protonated at a low pH condition (see Figures S3 and S4 of the Supporting Information).

Exploring Possible Drug Binding Sites Inside the BM2 Proton Channel. As for AM2, there have been a lot of studies concerning its drug binding sites.[31−36] Through the functional studies on the inhibition of the AM2 channel by AMT or RMT, Jing et al.[31] suggested that there were two distinct binding sites for AMT and RMT inside the AM2 channel. The solid-state NMR spectroscopy has confirmed that two drug binding sites could exist in the M2 proton channel and that the drug AMT exhibits different orientations at the two binding sites.[32] By performing a series of surface plasmon resonance (SPR) experiments measuring the affinity of AMT and RMT to the AM2 channel, Rosenberg et al.[33] probed the two possible binding sites. To investigate the two alternative binding sites of AMT and RMT inside the AM2 proton channel, Gu et al.[35] carried out MD simulations and PMF calculations and discovered that at intermediate pH conditions (pH ≈ 7.4), the surface binding site (S-binding) was less thermodynamically favorable than the pore binding (P-binding).

In order to explore possible drug binding sites in the BM2 channel, two representative BM2/AMT complex systems in the "bbbb" (low pH condition) and "dddd" (high pH condition) states were simulated for 30 ns. According to the backbone RMSD curves of the two systems, given in Figure S5 of the Supporting Information, the last 10 ns simulation trajectories were regarded as the equilibration stage and used for the data analysis. As shown in Figures 3a and Figure S6 of the Supporting Information, at different pH conditions, the AMT molecule stayed stably at different sites close to the N-terminal end. Basically, the pore radii of BM2 with AMT along the proton channel helix in the "bbbb" and "dddd" states exhibited similar behavior as that of the BM2 channel without the binding of AMT; see Figures 2b and 3b. In another words, the AMT molecule is of little effect on the pore radii of the BM2 channel, which is just sensitive to the pH condition.

Stouffer et al.[16] have suggested that the closed form of the AM2 channel is unable to bind AMT in its central cavity. Our study of the BM2 channel in the "dddd" state (high pH condition) reached the same conclusion; please see Figure 3a and Figure S6 of the Supporting Information. In the "bbbb" state (low pH condition), although the proton channel was widely open, we observed that the AMT molecule still stayed far away from His19, and water molecules were free to transport inside the channel such that the water wire was not

dx.doi.org/10.1021/jp309682t | J. Phys. Chem. B 2013, 117, 982−988

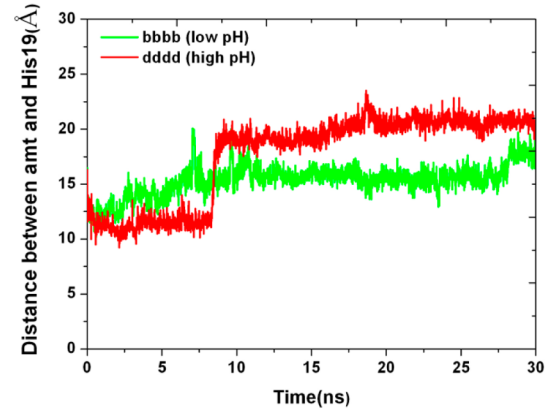

(a)

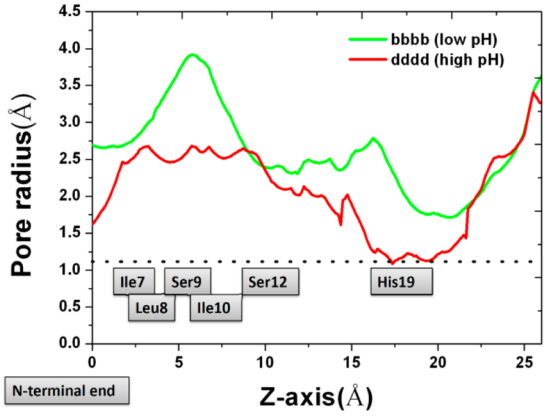

(b)

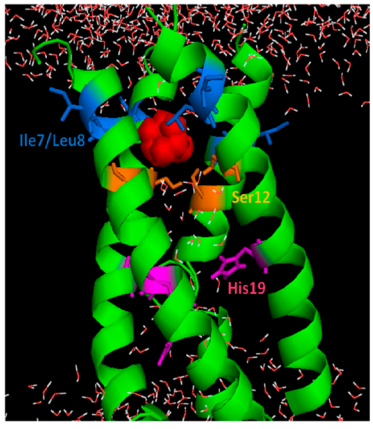

(c)

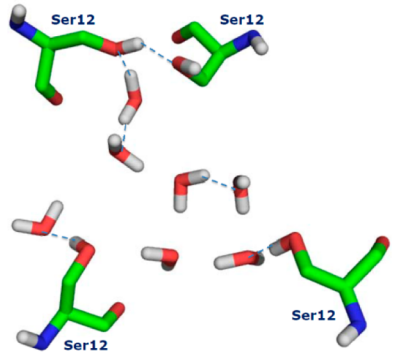

(d)

Figure 3. (a) Distance of mass centers between AMT and His19 and (b) the pore radius profile of the BM2 channel. The results were obtained from the equilibrated MD simulations of the BM2/AMT complex in two protonation states, "bbbb" (in green color) and "dddd" (in red color). (c) Average structure of the BM2/AMT complex in the "bbbb" state; the side chains of four His19 residues are represented by magenta sticks, and AMT is depicted as a red VDW sphere, and eight hydrophobic residues (Ile7 and Leu8) and four hydrophilic residues (Ser12) are represented by blue and orange sticks, respectively. (d) Hydrogen bonds are formed between Ser12 residues and water molecules, indicated by the blue dash line.

disrupted, which might result in the drug resistance of the BM2 channel to AMT; see Figure 3c and Figure S7 of the Supporting Information. From Figure 3c, we observed that the binding site of AMT to BM2 was located in the neighborhood of the hydrophobic core composed of the residues Ile7 and Leu8. Our results showed that the side chains of these hydrophobic residues (Ile7 and Leu8.) were poised away from the center of the channel helix, making room for the AMT docking as well as for the transportation of water molecules; in comparison, the analogous region (Val27 and Val28) in the AM2 channel is relatively narrow perhaps due to the arrangement of the side chains of Val27 and Val28. The side chains of four serine residues (Ser12) were poised toward the center of the channel helix, and a few hydrogen bonds were formed between water molecules and these serine residues (see Figure 3c,d), causing the decrease in the pore size of the region (see Figure 3b),

dx.doi.org/10.1021/jp309682t | J. Phys. Chem. B 2013, 117, 982−988

which set an obstacle for AMT to enter into the center pore on one hand and allowed water molecules to travel into the channel.

Additionally, we have monitored the dynamic behavior of the water molecules entering into the proton channel in the first a few nanoseconds, which is shown in Figure S7 of the Supporting Information. From the MD trajectory of the BM2/AMT complex in the "bbbb" state (low pH condition), we observed that from the C-terminal end, water molecules quickly entered the channel through the open His19 gate, and on the other side (N-terminal end), AMT competed with water molecules to enter into the proton channel pore; however, even in the presence of AMT, the water wire was still formed. From the plot of the water density changes against the simulation time, shown in Figure 4, we observed that as time evolved,

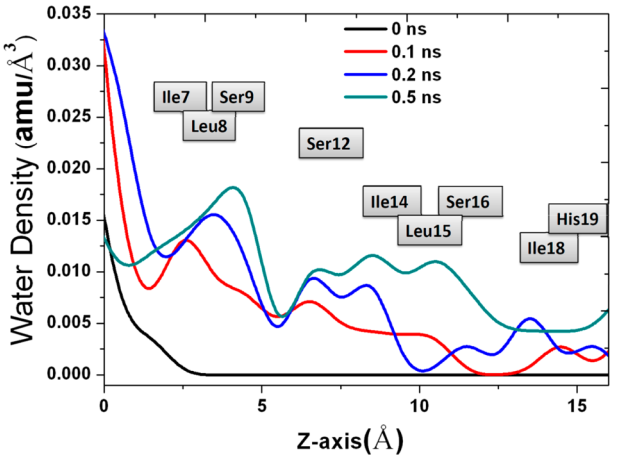

Figure 4. In the case of the BM2 channel in the "bbbb" state, the water density profile of the BM2 channel at different simulation times is shown, obtained from the MD simulation of the BM2/AMT complex.

water molecules were accumulated in two regions containing the same amino acid sequence, Ile-Leu-Ser. Thus, at low pH condition, a large room can be created for accommodating both AMT and water molecules, so that AMT cannot stop the formation of the water wire in the BM2 channel. On the contrary, the water wire may impede AMT into the center of the BM2 channel helix with the aid of the hydrogen bonding interaction between water molecules and four Ser12 residues.

Investigating Drug Resistance of BM2 through PMF Calculations. Basically, two distinct drug binding sites in the AM2 channel lead to two different drug inhibition mechanisms.[34] Stouffer et al.[16] have suggested that the drug binding inside the channel pore physically occludes the ion conductance pathway, but Schnell and Chou[17] have proposed that the drug binding outside of the channel pore should be associated with the inhibition of the AM2 ion channel. In addition, Yi et al.[37] have suggested that there is a second gate formed by Val27 playing a role in the inhibition of the AM2 proton channel by AMT.

Experimental studies[11] have shown that the S31N mutant of AM2 has resistance to the drug RMT. In comparison with the wild type (WT) of AM2, at low pH conditions, S31N mutant has the larger pore radii that may lead to the lower energy barriers for RMT to enter into or escape from the proton channel. The drug resistance of the AM2-S31N mutant may be ascribable to another aspect; there were fewer hydrogen bonds between the RMT and the His37 residues in the S31N mutant than that in the WT.[35] Qin et al.[36] found that AMT was located between Ser31 and Ala30 of the WT of AM2, but it was stabilized in a new position outside of the hydrophobic domain of the AM2-S31N mutant. Thus, the water wire was disrupted by RMT in the AM2 WT channel but was formed in the AM2-S31N mutant channel.

In order to energetically investigate the drug resistance of the BM2 channel at different pH conditions, we carried out PMF calculations for AMT entering into the BM2 proton channel pore from the N-terminal end. First, we compared the PMF results of AMT entering into the BM2 proton channel in different protonation states, such as "dddd" (high pH condition) and "bbbb" (low pH condition) states. An energy barrier of about 25 kcal/mol was observed for the AMT to arrive at His19 residues in the "dddd" state, in which the BM2 channel adopted a closed form. This indicates that it is very difficult for the AMT to get close to His19 residues at high pH conditions. In the "bbbb" state (low pH condition), the BM2 channel adopted an open form; therefore, it should be easy for AMT to enter into the center of the BM2 channel in the "bbbb" state, which was shown in our PMF results (see Figure 5a). As for the "bbbb" state, however, in the neighborhood of the hydrophobic core formed by Ile7 and Leu8 residues, an energy barrier of about 10 kcal/mol was calculated for AMT to arrive at the hydrophobic core (Ile7 and Leu8). The pore radius results have shown that the hydrophobic core is large enough for AMT to stay stably, but on the other hand, the pore is widely open for water molecules to move from one side to the other side. Particularly, with the aid of a number of hydrophilic residues (such as Ser9 and Ser12) close to the hydrophobic core (Ile7 and Leu8), hydrogen bonds were formed between those hydrophilic residues and water molecules. As we mentioned earlier, the hydrogen bonding interactions between the hydrophilic residues and water molecules may set the barrier for a drug movement inside the channel on one hand, and on the other hand, it may facilitate the formation of a water wire.

Furthermore, in the "bbbb" state (low pH condition), when the AMT was getting close to another hydrophobic core formed by Ile14 and Leu15, it had to overcome a series of energy barriers (about 6 kcal/mol in total). We observed that the four hydrophilic residues (Ser16) just were positioned below the hydrophobic core (Ile14 and Leu15). Similarly, the side chains of four serine residues (Ser16) were poised toward the center of the channel helix, playing the same role as that of the hydrophilic residues Ser9; see Figure S8 of the Supporting Information. It is intriguing that the energy barriers for AMT entering into the BM2 channel in the "bbbb" state (low pH condition) are associated with this structural element Ile-Leu-Ser (ILS) that is repeated twice in the amino acid sequence of BM2. The PMF results for RMT entering into the AM2 proton channel at neutral pH conditions have been given by Gu et al.,[35] indicating that RMT stayed close to the motif HxxxW region. In contrast, the PMF result of RMT entering the BM2 channel at low pH conditions, given in this study, showed that it was relatively difficult for RMT to arrive at the motif HxxxW region; see Figure 5b. This may be credited to the RMT size that is bigger than that of AMT; see Figure S9 of the Supporting Information.

■ CONCLUSION

In summary, MD simulations, in combination with the PMF calculations, have been carried out in this study, demonstrating

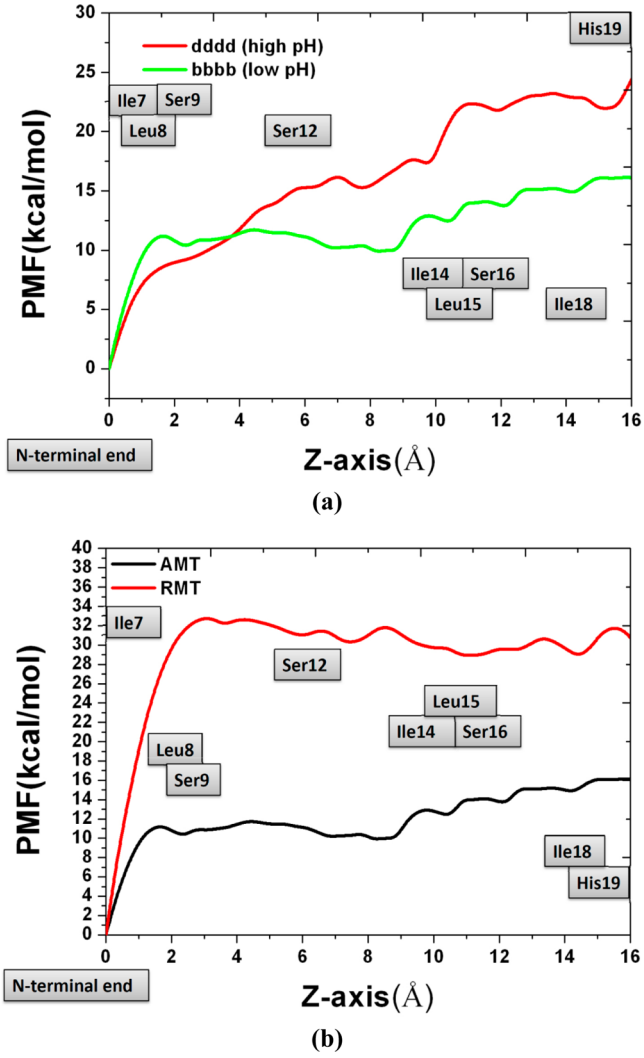

Figure 5. (a) PMF results for AMT entering into the BM2 proton channel pore from the N-terminal end in two protonation states, "bbbb" (in green color) and "dddd" (in red color). (b) PMF results for AMT (black) and RMT (red) entering into the BM2 proton channel pore from the N-terminal end in the "bbbb" state.

how the protonation states of His19 affect the structure and function of the BM2 proton channel and energetically explaining why the BM2 proton channel is resistant to AM2 inhibitors, AMT and RMT. First, we have shown that the pore size of the BM2 proton channel is sensitive to the protonation state of His19 residues, as well as the arrangement of His19 residues being protonated. Second, in either the presence or absence of the drug AMT, water wire could be formed at low pH conditions because a large space exists for the docking of AMT and the passing of water molecules in the hydrophobic region (Ile7 and Leu8) of the BM2 channel; on the other hand, the formation of the water wire sets a barrier for AMT entering into the center of the BM2 channel. Third, in comparison with the AM2 channel in which hydrophobic residues are dominant, the BM2 channel contains more hydrophilic residues, such as Ser9, Ser12, and Ser16; the hydrogen bonding interactions between water molecules and these hydrophilic residues may play roles in the formation of the water wire in the BM2 channel; moreover, it is interesting that these hydrophilic residues are separated by two or three hydrophobic residues in the amino acid sequence, forming a unique structural element (IL**S**xx**S**xIL**S**) in the BM2 channel. These unique arrangements (IL**S**xx**S**xIL**S**) would be of benefit to the transportation of water molecules inside the channel on one hand and set an obstacle to the movement of a drug into the channel on the other hand.

■ ASSOCIATED CONTENT

Supporting Information

Protonation states, RMSD curves, pore radius profiles, average structures, and snapshots of the complexes. This material is available free of charge via the Internet at http://pubs.acs.org.

■ AUTHOR INFORMATION

Corresponding Author

*E-mail: ghli@dicp.ac.cn.

Author Contributions

§These authors contributed equally.

Notes

The authors declare no competing financial interest.

■ ACKNOWLEDGMENTS

This work was supported by grants from the national high technology research and development program of China (863 project) (No. 2012AA01A305), the National Science Foundation of China under Contract No. 31070641/C050101, and the National Basic Research Program of China (973) under Contract 2012CB721002. We acknowledge Guangrong Qin and Kunqian Yu for suggestions about molecular modeling. We also thank Jinan Wang for important help and insightful discussions. At last, Dinglin Zhang should not be forgotten for software and computational support.

■ REFERENCES

(1) Wang, J.; Pielak, R. M.; McClintock, M. A.; Chou, J. J. *Nat. Struct. Mol. Biol.* **2009**, *16*, 1267−1271.

(2) Rouse, S. L.; Carpenter, T.; Stansfeld, P. J.; Sansom, M. *Biochemistry* **2009**, *48*, 9949−9951.

(3) Pinto, L. H.; Lamb, R. A. *J. Biol. Chem.* **2006**, *281*, 8997−9000.

(4) Paterson, R. G.; Takeda, M.; Ohigashi, Y.; Pinto, L. H.; Lamb, R. A. *Virology* **2003**, *306*, 7−17.

(5) Pinto, L. H.; Dieckmann, G. R.; Gandhi, C. S.; Papworth, C. G.; Braman, J.; Shaughnessy, M. A.; Lear, J. D.; Lamb, R. A.; Degrado, W. F. *Proc. Natl. Acad. Sci. U.S.A.* **1997**, *94*, 11301−11306.

(6) Pielak, R. M.; Chou, J. J. *Biochim. Biophys. Acta* **2011**, *1808*, 522−529.

(7) Cross, T. A. *Nat. Struct. Mol. Biol.* **2009**, *16*, 1207−1209.

(8) Hatta, M.; Goto, H.; Kawaoka, Y. *J. Virol.* **2004**, *78*, 5576−5583.

(9) Helenius, A. *Cell* **1992**, *69*, 577−578.

(10) Wang, C.; Takeuchi, K.; Pinto, L. H.; Lamb, R. A. *J. Virol.* **1993**, *67*, 5585−5594.

(11) Pielak, R. M.; Schnell, J. R.; Chou, J. J. *Proc. Natl. Acad. Sci. U.S.A.* **2009**, *106*, 7379−7384.

(12) Mould, J. A.; Paterson, R. G; Takeda, M.; Ohigashi, Y.; Venkataraman, P.; Lamb, R. A.; Pinto, L. H. *Dev. Cell* **2003**, *5*, 175−184.

(13) Hu, F.; Luo, W.; Hong, M. *Science* **2010**, *330*, 505−508.

(14) Sharma, M.; Yi, M.; Dong, H.; Qin, H.; Peterson, E.; Busath, D. D.; Zhou, H.-X.; Cross, T. A. *Science* **2010**, *330*, 509−512.

(15) Pielak, R. M.; Chou, J. J. *J. Am. Chem. Soc.* **2010**, *132*, 17695−17697.

(16) Stouffer, A. L; Acharya, R.; Salom, D.; Levine, A. S.; Di Costanzo, L.; Soto, C. S.; Tereshko, V.; Nanda, V.; Stayrook, S.; Degrado, W. F. *Nature* **2008**, *451*, 596−600.

(17) Schnell, J. R; Chou, J. J. *Nature* **2008**, *451*, 591−595.

(18) Kandt, C.; Ash, W. L.; Tieleman, D. P. *Methods* **2007**, *41*, 475−488.

(19) Faraldo-Gomez, J. D.; Smith, G. R.; Sansom, M. *Eur. Biophys. J.* **2002**, *31*, 217−227.
(20) Jorgensen, W. L; Chandrasekhar, J.; Madura, J. D.; Impey, R. W.; Klein, M. L. *J. Chem. Phys.* **1983**, *79*, 926−935.
(21) Der Spoel, D. V.; Lindahl, E.; Hess, B.; Groenhof, G.; Mark, A. E.; Berendsen, H. J. *J. Comput. Chem.* **2005**, *26*, 1701−1718.
(22) Siu, S. W.; Vacha, R.; Jungwirth, P.; Bockmann, R. A. *J. Chem. Phys.* **2008**, *128*, 125103.
(23) Hess, B.; Bekker, H.; Berendsen, H. J. C.; Fraaije, J. G. E. M. *J. Comput. Chem.* **1997**, *18*, 1463−1472.
(24) Darden, T.; York, D.; Pederson, L. *J. Chem. Phys.* **1993**, *98*, 10089.
(25) Schüttelkopf, A. W.; van Aalten, D. M. F. *Acta. Crystallogr., Sect. D* **2004**, *60*, 1355−1363.
(26) Chew, C. F.; Guy, A.; Biggin, P. C. *Biophys. J.* **2008**, *95*, 5627−5636.
(27) Torrie, G. M.; Valleau, J. P. *J. Comput. Phys.* **1977**, *23*, 187−199.
(28) Kumar, S.; Rosenberg, J.; Bouzida, D.; Swendsen, R. H.; Kollman, P. A. *J. Comput. Chem.* **1992**, *13*, 1011−1021.
(29) Smart, O. S.; Neduvvelil, J. R.; Wang, X.; Wallace, B. A.; Sansom, M. *J. Mol. Graphics* **1996**, *14*, 354−360.
(30) Khurana, E.; Peraro, M. D.; DeVane, R.; Vemparala, S.; DeGrado, W. F.; Klein, M. L. *Proc. Natl. Acad. Sci. U.S.A.* **2009**, *106*, 1069−1074.
(31) Jing, X.; Ma, C.; Ohigashi, Y.; Oliveira, F. A.; Jardetzky, T. S.; Pinto, L. H.; Lamb, R. A. *Proc. Natl. Acad. Sci. U.S.A.* **2008**, *105*, 10967−10972.
(32) Cady, S. D.; Schmidt-Rohr, K.; Wang, J.; Soto, C. S.; DeGrado, W. F.; Hong, M. *Nature* **2010**, *463*, 689−692.
(33) Rosenberg, M. R.; Casarotto, M. G. *Proc. Natl. Acad. Sci. U.S.A.* **2010**, *107*, 13866−13871.
(34) Ohigashi, Y.; Ma, C.; Jing, X.; Balannik, V.; Pinto, L. H.; Lamb, R. A. *Proc. Natl. Acad. Sci. U.S.A.* **2009**, *106*, 18775−18779.
(35) Gu, R.; Liu, L. A.; Wei, D.; Du, J.; Liu, L.; Liu, H. *J. Am. Chem. Soc.* **2011**, *133*, 10817−10825.
(36) Qin, G.; Yu, K.; Shi, T.; Luo, C.; Li, G.; Zhu, W.; Jiang, H. *J. Phys. Chem. B* **2010**, *114*, 8487−8493.
(37) Yi, M.; Cross, T. A.; Zhou, H. X. *J. Phys. Chem. B* **2008**, *112*, 7977−7979.